Direct and Diffuse Radiation in the Shallow Cumulus–Vegetation System: Enhanced and Decreased Evapotranspiration Regimes

X. PEDRUZO-BAGAZGOITIA

Meteorology and Air Quality Group, Wageningen University and Research, Wageningen, Netherlands

H. G. OUWERSLOOT

Atmospheric Chemistry Department, Max Planck Institute for Chemistry, Mainz, Germany

M. SIKMA AND C. C. VAN HEERWAARDEN

Meteorology and Air Quality Group, Wageningen University and Research, Wageningen, Netherlands

C. M. J. JACOBS

Climate Change and Adaptive Land and Water Management, Wageningen University and Research, Wageningen, Netherlands

J. VILÀ-GUERAU DE ARELLANO

Meteorology and Air Quality Group, Wageningen University and Research, Wageningen, Netherlands

ABSTRACT

Guided by a holistic approach, the combined effects of direct and diffuse radiation on the atmospheric boundary layer dynamics over vegetated land are investigated on a daily scale. Three numerical experiments are designed that are aimed at disentangling the role of diffuse and direct radiation below shallow cumulus at the surface and on boundary layer dynamics. A large-eddy simulation (LES) model coupled to a land surface model is used, including a mechanistically immediate response of plants to radiation, temperature, and water vapor deficit changes. The partitioning in direct and diffuse radiation created by clouds and farther inside the canopy is explicitly accounted for. LES results are conditionally averaged as a function of the cloud optical depth. The findings show larger photosynthesis under thin clouds than under clear sky, due to an increase in diffuse radiation and a slight decrease in direct radiation. The reduced canopy resistance is the main driver for the enhanced carbon uptake by vegetation, while the carbon gradient and aerodynamic effects at the surface are secondary. Because of the coupling of CO_2 and water vapor exchange through plant stomata, evapotranspiration is also enhanced under thin clouds, albeit to a lesser extent. This effect of diffuse radiation increases the water use efficiency and evaporative fraction under clouds. The dynamic perturbations of the surface fluxes by clouds do not affect general boundary layer or cloud characteristics because of the limited time and space where these perturbations occur. It is concluded that an accurate radiation partitioning calculation is necessary to obtain reliable estimations on local surface processes.

---

1. Introduction

The atmospheric boundary layer (ABL) dynamics are strongly influenced by the surface–atmosphere exchange of heat and moisture, which, over vegetated land, is conditioned by CO_2 concentration. Variations in atmospheric conditions due to turbulent motions locally modify surface fluxes at scales within a few hundreds of meters in the horizontal (Huang and Margulis 2010),

and modify the spatial average latent and sensible heat fluxes at regional scales (between 10 and 50 km). These interactions are representative of the so-called land–atmosphere feedbacks. As an illustrative example of the role of dynamics on such a large-scale coupling, De Bruin et al. (1989) already found that warm and dry entrained air was critical for sustaining high evaporation rates at the surface. Van Heerwaarden et al. (2009) presented an overview of the factors within the ABL affecting evapotranspiration. The heterogeneities of the surface characteristics, or static heterogeneities, add to the complexity of land–atmosphere interactions by varying air temperature (Baldocchi and Ma 2013) and the surface fluxes at a scale of several kilometers (Avissar and Schmidt 1998; Esau and Lyons 2002). At a regional scale, such surface heterogeneities have the potential to trigger secondary circulations (Garcia-Carreras et al. 2010).

A key factor that affects plant activity is the partitioning of radiation into direct and diffuse components, which depends on the transfer of radiation through the atmosphere, influenced by clouds and aerosols and through the canopy itself. Canopies convert radiation from direct to diffuse by the scattering of light with leaves (Goudriaan 1977; Norman 1979). Aerosols and clouds are known to decrease total radiation and increase the diffuse fraction through light scattering. Barbaro et al. (2014) showed the relevant impact of aerosol–radiation interactions on the boundary layer, but did not consider the effect that diffuse radiation would exert on the vegetated canopy. Diffuse radiation is known to increase the carbon (from here on representing only carbon from CO_2) assimilation of vegetated canopies (Kanniah et al. 2012) due to a more homogeneous spread of radiation in the canopy, thus reducing the saturation of leaves at the top of the canopy and increasing the available radiation at the bottom and shaded parts of the canopy. Min and Wang (2008) found increased CO_2 uptake by plants for conditions with an atmospheric transmittance index below 1, which favor the scattering of radiation and promote diffuse radiation. An increase in carbon uptake over forests and under shallow cumulus clouds has been reported by several studies (Betts et al. 1999; Freedman et al. 2001; Oliphant et al. 2011) in spite of a reduction of global radiation. Since the vegetation–atmosphere system couples water and carbon cycles through photosynthesis, evapotranspiration and sensible heat flux exchanges are also affected by diffuse radiation (Wang et al. 2008; Oliveira et al. 2011).

Similar to aerosols, clouds also influence the partitioning between direct and diffuse radiation. However, the optical thickness of clouds can be larger than that for aerosols. Thick clouds absorb most direct radiation (Min 2005), and little diffuse radiation reaches the surface.

Below optically thin clouds the reduction in direct radiation can be significant but limited, and diffuse radiation is greatly enhanced (Cheng et al. 2016). We here follow the convention by Min (2005), where thin clouds are defined as the ones with cloud optical depth $\tau < 8$ and thick clouds for larger τ. The motivation was that clouds with $\tau > 8$ did not allow any direct radiation go through. Similarly, Cheng et al. (2016) set the threshold at $\tau = 7$. As we found in our study, however, such thresholds vary during the day, thus making the definition of thin and thick clouds quite arbitrary.

Convective clouds impose some additional effects on surface–atmosphere interactions compared to aerosols. Their onset, development, and characteristics depend on surface conditions (Golaz et al. 2001; Garcia-Carreras et al. 2011; Chlond et al. 2014). They are known to vent air from the boundary layer to higher layers, reducing the momentum, moisture, and subcloud-layer growth (Betts 1973; Neggers et al. 2006), thereby altering the surface fluxes. More important to our study are the dynamic heterogeneities created at the surface by (inhomogeneous) cloud shading. As a result, clouds disrupt the surface energy balance by modifying surface temperature and specific humidity, creating inhomogeneities that vary the turbulent mixing near the surface. Lohou and Patton (2014) found a higher evaporative fraction (EF) on shaded surface because the latent heat flux (LE) decreased less compared to the sensible heat flux (SH). The shade-induced energy reduction at the surface promotes the narrowing of space between updrafts and, subsequently, the reduction of intercloud distance (Horn et al. 2015). Moreover, Gronemeier et al. (2017) found that cloud shading is able to generate secondary circulations, although its strength and significance depend on the solar zenith angles.

Most of these studies were idealized numerical experiments designed to disentangle the complexity of the cloud–surface interactions and assumed free convective conditions with an instantaneous surface response. None of them, however, considered explicitly the impact of direct and diffuse radiation on active vegetation at the surface. This possibility poses interesting questions, such as whether the local impact of radiation partitioning by clouds on vegetation has a domain-averaged effect, given the distinct responses for thin and thick clouds, or, in addition, whether the direct–diffuse partitioning of radiation near the surface ultimately influences the characteristics of boundary layer clouds themselves.

To our knowledge, no systematic study on the impact of shortwave direct and diffuse radiation (SW_{dir} and SW_{dif}, respectively), created both in clouds and within the canopy, on the boundary layer dynamics has been performed. Current developments in cloud observation

(Schwartz et al. 2017) allow extensive studies on individual clouds, variability of cloud optical depth and solar irradiance within clouds and its effect on vegetation carbon uptake (Cheng et al. 2016). These advancements call for a similar procedure in explicit numerical simulations, where the impacts of varying cloud optical depths at the surface are considered by performing systematic numerical experiments. The large-eddy simulation (LES) technique, with horizontal resolution on the order of 50 m, has the capability to explicitly simulate shallow clouds and its spatial variability in cloud thickness (Vilà-Guerau de Arellano et al. 2014; Horn et al. 2015). A novel aspect of our LES study is the coupling to a land surface model aware of both direct and diffuse radiation, leading to an integrated approach where diffuse radiation is explicitly treated both at the clouds and inside the canopy. The land surface model uses a plant physiological scheme, including a mechanistic model for stomatal aperture, to account for very fast fluctuations (on the order of seconds) in diffuse and direct radiation and, thus, subsequent modifications on the carbon and water vapor exchanged between the vegetation and the atmosphere (Jacobs and de Bruin 1997; Ronda et al. 2001). We perform systematic simulations where we use a radiative scheme to explicitly account for the direct and diffuse radiation generated by clouds, coupled to a canopy scheme where direct and diffuse radiation are treated explicitly. Such a high detail of CO_2 processes at the surface also allows us to further investigate the relation between clouds and the carbon cycle (Vilà-Guerau de Arellano et al. 2012) at daily scales. With the high spatial resolution of our numerical experiments, we are able to quantify the subgrid variability of larger-scale models, for example, the Integrated Forecast System (IFS), with similar mechanistic formulations for photosynthesis and stomatal conductance (Boussetta et al. 2013). The domain, on the order of $24 \times 24 \, km^2$, is representative of a typical grid box for regional carbon–climate models.

Aiming to shed light on the issues posed above, the research questions of this study are the following:

- Does direct and diffuse radiation modulation by shallow cumulus affect evapotranspiration and CO_2 assimilation locally? And over the whole domain? How does this impact the partitioning of sensible and latent heat flux?
- Under these nonstationary surface conditions, do the direct and diffuse radiation alterations from clouds feed back into boundary layer dynamics? Do cloud characteristics depend on it too?

The remaining part of this study is structured as follows: section 2 describes the methodology and tools used for this study, including the implementation of a canopy radiative transfer scheme accounting for direct and diffuse radiation, as well as the research strategy. Section 3 contains the main findings and points of discussion of our analysis. Finally, the concluding summary of the research and recommendations are provided in section 4.

2. Methods and numerical experiments

a. Explicit simulation of the coupling: DALES

The Dutch Atmospheric Large-Eddy Simulation (DALES) has been under continuous development since the 1980s (Nieuwstadt and Brost 1986; Heus et al. 2010; Böing et al. 2012; Ouwersloot et al. 2017). It incorporates an interactive land surface scheme responding to atmospheric processes described in Jacobs and de Bruin (1997), van Heerwaarden et al. (2010), and Vilà-Guerau de Arellano et al. (2015). Within the land surface scheme, we use the plant physiological model A-gs (Jacobs and de Bruin 1997) to simulate the behavior of vegetation and assuming an instantaneous response of vegetation to atmospheric and radiation forcings. This study uses DALES, version 4.1, with additional upgrades concerning the radiation transfer within the canopy [section 2c(2)] and conditional sampling at the surface (section 2d). We present here the most relevant parts of the land surface model, that is, the contribution of vegetation to latent heat flux, the sensible heat flux, and the carbon assimilation rate by vegetation.

The contribution of vegetation to total latent heat flux is given by

$$\mathrm{LE}_{\mathrm{veg}} = c_{\mathrm{veg}} \frac{\rho L_v}{r_a + r_{\mathrm{veg}}} [q_{\mathrm{sat}}(T_s) - q], \qquad (1)$$

where c_{veg} is the vegetation cover fraction, ρ stands for the air density, and L_v is the specific latent heat constant for evaporation. The specific humidity and saturated specific humidity are given by q and q_{sat}, respectively, and the surface temperature is given by T_s. The vegetation canopy resistance r_{veg}, giving the capacity of stomata (upscaled at canopy level) to exchange water vapor with the environment, is obtained by $r_{\mathrm{veg}} = 1/g_c$, where g_c represents the stomatal conductance at canopy level. Further information on its calculation is given in section 2c(2) and in the supplemental material. Since the vegetation cover is 90%, leaving only 10% for bare soil, $\mathrm{LE}_{\mathrm{veg}}$ is the main contributing term to the total latent heat flux (LE).

The sensible heat flux is calculated by

$$\mathrm{SH} = \frac{\rho c_p}{r_a} (\theta_s - \theta_{\mathrm{air}}), \qquad (2)$$

where c_p is the specific heat capacity of air at constant pressure, θ_s is the surface potential temperature, and θ_{air}

is the potential temperature of the first level above the surface.

The carbon assimilated through photosynthesis by the vegetation canopy per second A_n is related to the vegetation resistance by

$$A_n = \frac{C_s - C_i}{r_a + r_{\text{veg}_{CO_2}}}, \tag{3}$$

where C_s and C_i are the external and internal CO_2 concentrations, respectively, and r_a and $r_{\text{veg}_{CO_2}}$ the aerodynamic and vegetation canopy resistance for CO_2 exchange, respectively, where $r_{\text{veg}_{CO_2}} = 1.6\, r_{\text{veg}}$. The factor of 1.6 accounts for the different molecular diffusivity of water vapor and CO_2 in the air (Jacobs and de Bruin 1997).

For a detailed description on the treatment of direct and diffuse radiation in the canopy resistance calculations, the reader is referred to the supplemental material.

b. Conceptual analysis: CLASS

To support the analysis of the results in DALES, in section 3a(2) we make use of the Chemistry Land-Surface Atmosphere Soil Slab (CLASS) model (Vilà-Guerau de Arellano et al. 2015). This box model is based on the mixed-layer equations to obtain the temporal evolution of the boundary layer and surface processes. The land surface model in CLASS (van Heerwaarden et al. 2010) is similar to that of DALES, and the schemes described in sections 2c(1) and 2c(2) are also present and used in CLASS. With this box model we analyze the response of vegetation to temporal changes in cloud optical depth and radiation in a more controlled environment than in DALES, where explicit turbulence makes interpretation difficult. By using CLASS, it is easier to fix the surface conditions and untangle the effects of different factors affecting carbon assimilation. We prescribe the onset, duration, and disappearance of a cloud in CLASS by prescribing the cloud optical depth for each time step.

c. Direct and diffuse radiation partitioning

To account for shortwave direct and diffuse radiation, we first divide the atmosphere in two layers, separated at a height of 500 hPa. Above this level we consider a nonpolluted standard Rayleigh atmosphere (Barbaro et al. 2014). We assume Rayleigh scattering to be the dominant scattering process because of the molecules present at these altitudes. Since our goal is to understand the explicit effect of direct and diffuse radiation generated by shallow cumulus, we assume all radiation at the top of the domain to be direct unless stated otherwise in the experiment. By doing this, we isolate the added contribution of cloud-generated diffuse radiation at the top of the canopy. We prescribe a maximum value of $SW_{\text{dir}}^{\text{ToD}} = 1000\, W\, m^{-2}$ (unless stated otherwise) as a top boundary condition in the domain, which is a representative value for the downward shortwave radiation at the height of 500 hPa (Barbaro 2015). To confirm the validity of the results, we design an additional experiment (AER; section 2e) with a combination of direct and diffuse radiation at the top of the domain. We explicitly simulate the shortwave radiative transfer between the 500-hPa level and the surface. Concerning longwave radiation, only the upward and downward components at the surface are calculated, according to

$$LW^{\uparrow} = \varepsilon_s \sigma \theta_s^4 \quad \text{and} \tag{4}$$

$$LW^{\downarrow} = \varepsilon_{\text{air}} \sigma \theta_{\text{air}}^4, \tag{5}$$

where the emissivities for surface and air are $\varepsilon_s = 1$ and $\varepsilon_{\text{air}} = 0.8$, respectively, and σ is Boltzmann's constant. This is necessary to obtain realistic radiation and surface balances at the surface. Thus, we do not account for longwave radiation from clouds or different gas concentrations, as we focus on the radiative transfer of shortwave radiation and do not expect significant differences in the longwave components between experiments.

1) RADIATIVE TRANSFER IN CLOUDS: DELTA-EDDINGTON APPROXIMATION

The Eddington method for shortwave radiative transfer was originally proposed by Shettle and Weinman (1970) and later approximated and further developed including a delta function by Joseph et al. (1976). This method has been already expanded for aerosols and successfully tested in DALES by Barbaro et al. (2014).

The delta-Eddington calculates the transfer of radiation with the following governing equations:

$$SW_{\text{dif}}^{\uparrow} = I_0(\tau') - \frac{2}{3} I_1(\tau'), \tag{6}$$

$$SW_{\text{dif}}^{\downarrow} = I_0(\tau') + \frac{2}{3} I_1(\tau'), \quad \text{and} \tag{7}$$

$$SW_{\text{dir}}^{\downarrow} = \mu F_0 e^{-\tau'/\mu}, \tag{8}$$

where τ' refers to the optical (cloud) depth after applying the delta-Eddington approximation that assumes most of the scattering to be forward; SW stands for [upward ($\uparrow$) or downward ($\downarrow$) and direct (dir) or diffuse (dif)] shortwave radiation; $\mu = \cos\theta$, where θ is the zenith angle; and F_0 is the solar radiative flux perpendicular to the incidence direction at the top of the domain. The Eddington assumption supposes that we can decompose the total diffuse radiation I_{dif} as a superposition of two functions I_0 and I_1, such that they fulfill $I_{\text{dif}}(\tau) = I_0(\tau) + \mu I_1(\tau)$ (Shettle and Weinman 1970). The
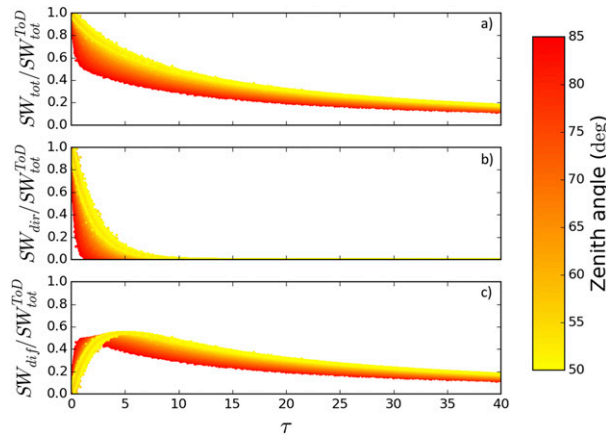
FIG. 1. Ratio of (a) total, (b) direct, and (c) diffuse radiation at the surface to the total radiation at the top of the domain SW_{top}^{ToD} as a function of τ obtained from the REF experiment. The gradual color shows the dependency on solar zenith angle, ranging from $\theta = 50°$ (yellow) at its zenith for the experiment day to $\theta = 85°$ (red).

shape of I_0 and I_1 for different cases is given in Shettle and Weinman (1970). It must be noted that the delta-Eddington method is sensitive to the solar angle, as shown in Fig. 1. Here we assume the shadow of a cloud to be always right below the cloud, although we account for the solar angle dependences in the delta-Eddington calculations and in the radiation intensity at the top of the domain. This is a reasonable approximation according to Schumann et al. (2002), who found shadow asymmetries due to nonzero solar zenith angle to be irrelevant for turbulent motions in the boundary layer. We fix the effective radius of droplets to be $r_{eff} = 0.01$ mm, a typical droplet size for shallow cumulus (Baker and Latham 1979). This is relevant for obtaining the cloud optical depth based on the liquid water content, where we follow Stephens (1984). We performed a sensitivity analysis on the impact of the droplet effective radius on shortwave radiation and found little impact within the range typical for cumulus clouds (Lu et al. 2013) (results not shown).

For a complete explanation and derivation of the delta-Eddington method, the reader is referred to Shettle and Weinman (1970) for the original Eddington method, to Joseph et al. (1976) for the delta-Eddington approximation, and to Heus et al. (2010) and Barbaro et al. (2014) for its application.

2) RADIATIVE TRANSFER IN CANOPY: GAUSSIAN METHOD

The limitation of single big leaf models, like applied by Vilà-Guerau de Arellano et al. (2014), to account for canopy radiative transfer is tackled by explicitly calculating radiation profiles for direct and diffuse radiation.

This is especially relevant for the current work, where both diffuse and direct radiation components are accurately calculated at the top of the canopy. To this end, we employ the scheme used by Jacobs and de Bruin (1997) and inspired from the radiative transfer approximations used in Goudriaan (1977) and adapted by Spitters (1986). A detailed description of the canopy radiative transfer and canopy upscaling is given in the supplemental material. In short, the main characteristics of the scheme are the following:

- Diffuse radiation has a (constant) extinction coefficient inside the canopy that is smaller (for most of the day) than that of the (solar angle dependent) direct radiation.
- The direct radiation that is not transmitted nor absorbed is scattered by leaves or the ground and converted into diffuse radiation inside the canopy.
- Leaves are distributed spherically in the canopy and affect the radiation penetration accordingly.

Total stomatal conductance is obtained at three levels inside the canopy after calculating the radiation profiles and the amount of shaded and sunlit leaves per level. For the calculations of stomatal conductance at leaf level, we use the A-gs model described by Jacobs et al. (1996) and Jacobs and de Bruin (1997). Bulk stomatal conductance of CO_2 for the canopy is obtained through the Gaussian integration method described in Goudriaan (1986) and implemented in the IFS model by the European Centre for Medium-Range Weather Forecasts (ECMWF; Boussetta et al. 2013). As in other studies (Jacobs and de Bruin 1997; Boussetta et al. 2013), we assume that radiation transfer is the most relevant factor throughout the canopy. Thus, we use bulk values for other dynamic variables such as leaf temperature, vapor pressure deficit, or CO_2 mixing ratio, and keep them invariable throughout the canopy. Multilayer canopy models that have to resolve the surface energy balance and all dynamic variables at each canopy level are computationally more expensive. As a result, our approach is faster, while still considering radiation variations within the canopy.

d. Conditional averaging

The alteration in radiation by clouds affects the surface locally (Horn et al. 2015). It is therefore convenient to apply a two-dimensional conditional averaging of surface properties dependent on cloud properties above. We classify the surface response according to cloud optical depth in bins of gradually increasing width: bins of 0.5 width between values of cloud optical depth $\tau = 0$ and $\tau = 5$, and in bins of 1.0 width between values of $\tau = 5$ and $\tau = 10$ to obtain more information on the

properties at the surface for cloud optical depths typical of shallow cumulus clouds (McFarlane and Grabowski 2007; Slawinska et al. 2008). Three more bins are defined for thicker clouds: two bins with a width of 5.0 between $10 < \tau \leq 15$ and $15 < \tau \leq 20$ and a bin for $\tau > 20$.

Since we are also interested in the properties of the clouds during the experiment, we make further use of a three-dimensional conditional average over the grid, similar to that used in other studies (Siebesma et al. 2003; Ouwersloot et al. 2013; Sikma and Ouwersloot 2015). In this case, we mainly focus on the conditional averages for clouds (liquid water mixing ratio $q_l > 0$) and for the buoyant part of clouds or cloud cores ($q_l > 0$ and virtual potential temperature $\theta_v > \overline{\theta}_v$), where the overbar stands for domain average properties at each vertical level.

e. Research strategy

We reproduce a representative warm and initially clear early autumn day of September in the Netherlands developing a convective boundary layer. Surface and upper observations are initially obtained from observations at the Cabauw Experimental Site for Atmospheric Research (CESAR). The case has been adapted to allow the onset of active shallow cumulus (Vilà-Guerau de Arellano et al. 2014). First, shallow cumulus develops between 1000 and 1100 UTC, after which a maximum cloud cover of ~20% is reached between 1300 and 1500 UTC. The numerical experiments simulate 10 h, from 0700 to 1700 UTC (0900 to 1900 local time), with an initially well-mixed boundary layer of around 120 m and with no prescribed horizontal wind. We define the boundary layer height as the height at which the gradient in potential temperature θ equals 50% of the maximum vertical gradient (Ouwersloot et al. 2011). We make use of an all-or-nothing microphysics scheme, assuming condensation of all specific humidity above local saturation point and none if saturation is not reached. The surface consists of a homogeneous grassland of leaf area index (LAI) equal to 2 with radiative and dynamic properties typical of short grass, and a vegetation cover of 90%. The domain is $24 \times 24 \times 5.4 \, \text{km}^3$ with a gridbox size of $50 \times 50 \times 12 \, \text{m}^3$. Such a vertical resolution ensures the explicit resolution of clouds and its dynamics.

We design three experiments: reference or control (REF), direct (DIR), and diffuse (DIF). The REF experiment calculates the amount of direct and diffuse radiation below the clouds using the delta-Eddington approximation [section 2c(1)] and sets the response of the surface to radiation through the canopy scheme as described in section 2c(2) and with more detail in the supplemental material. The DIR experiment uses the same radiation below the cloud, but treats all radiation reaching the canopy as direct radiation. In turn, the DIF experiment considers all radiation reaching the canopy to

be diffuse as long as there is a cloud above. With these three experiments, we explore the sensitivity of the surface and boundary layer to the direct radiation and diffuse radiation ratio below clouds. Two additional experiments are carried out to put the aforementioned numerical experiments in perspective. The first one (AER) mimics the effect of downward diffuse radiation due to Rayleigh scattering above the domain by converting 7% of the direct radiation SW_{dir}^{ToD} to diffuse radiation SW_{dif}^{ToD} at the top of the domain (Barbaro et al. 2014). This radiative effect at the surface is similar to that of a boundary layer with clouds and a significant presence of light-scattering aerosols (Yu et al. 2002; Barbaro et al. 2014). The second experiment is identical to the reference experiment but with a leaf area index of 5 (LAI5). The goal of this experiment is to reveal the sensitivity of the surface–boundary layer system to a change in vegetation density, which impacts the penetration of direct and diffuse radiation in the canopy and, thus, the surface fluxes.

3. Results and discussion

a. Impact of shallow cumulus at surface

1) IMPACT ON SURFACE FLUXES

Figure 1b shows the exponential decay in shortwave direct radiation, as stated in Eq. (8). There is a solar-angle-dependent maximum in diffuse radiation for τ between $\tau = 1$ and $\tau = 8$ (Fig. 1c). Increasing cloud thickness converts more direct to diffuse radiation, while at the same time reduces the overall radiation going through the cloud (Fig. 1a). This increase in diffuse fraction is of critical importance for the feedbacks and interactions in our numerical experiments, since the cloud optical depth of the shallow cumulus created during the day ranges around those values. In fact, McFarlane and Grabowski (2007) observed that in the tropics the optical depth of the most common shallow cumulus ranges between $\tau = 5$ and $\tau = 10$, a finding also supported through numerical experiments by Slawinska et al. (2008). To our knowledge, such a study on typical optical thickness of shallow cumulus has not been carried out for midlatitudes, where our study focuses. The results shown in Fig. 1 are consistent with the satellite measurements by Cheng et al. (2016), supporting the use of a broadband radiation scheme like the delta-Eddington for our purposes.

The perturbation of radiation by clouds has an immediate effect at the surface turbulent fluxes. The presence of any cloud locally reduces the total radiation at surface, from around 15% for very thin clouds ($\tau < 3$) to almost 85% for very deep clouds ($\tau \sim 40$; Fig. 1a). In our study we focus on the effect of shallow cumulus. Thus, we pay special attention to clouds with $\tau < 8$. Figure 2 depicts the
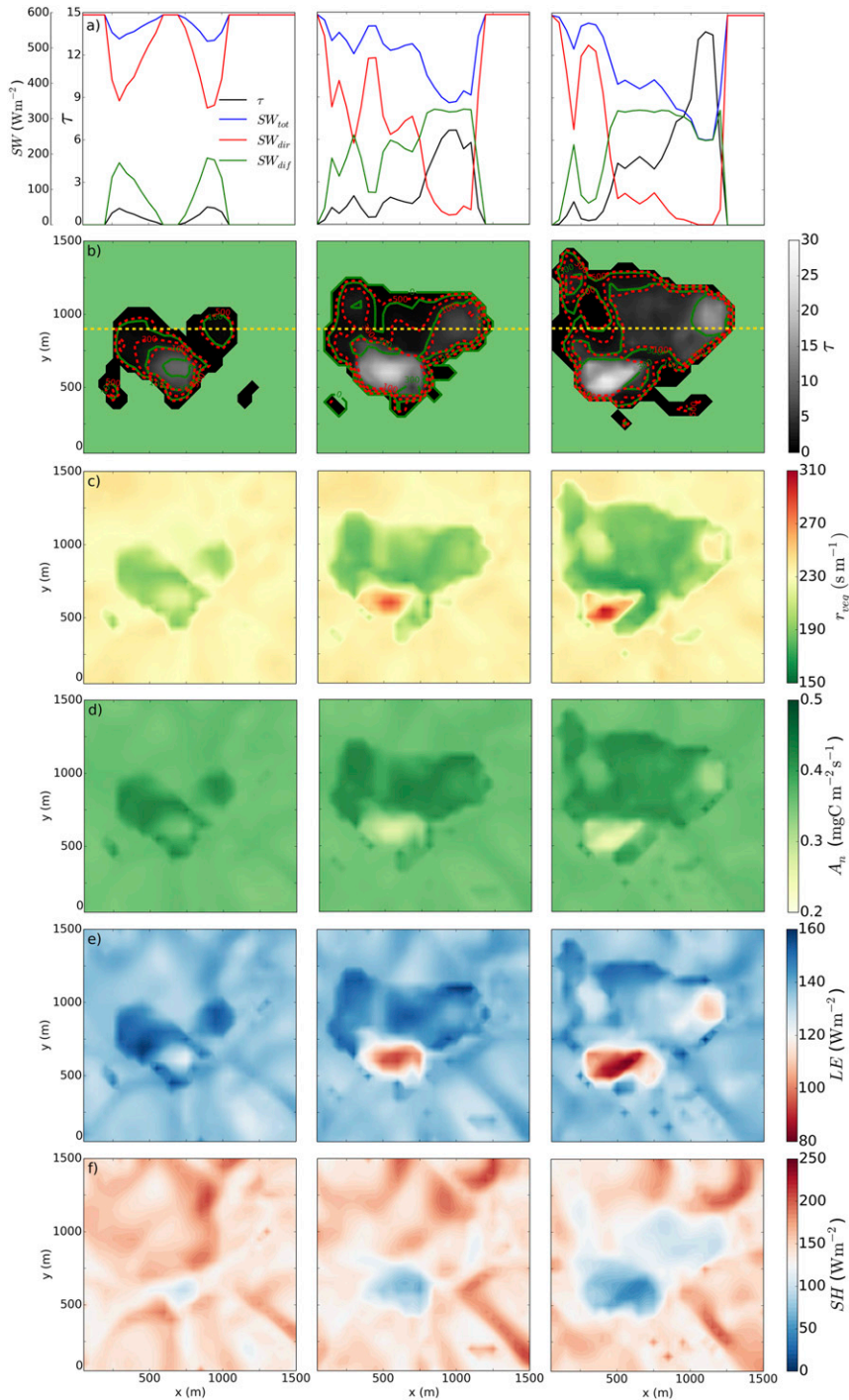
FIG. 2. (a) Values of cloud optical depth τ (black), shortwave direct SW_{dir} (red), shortwave diffuse SW_{dif} (green), and total radiation SW_{tot} (blue) along the cross section (horizontal yellow dashed line) displayed in (b). (b) Instantaneous horizontal cross sections of τ (shaded) with SW_{dir} (dashed red) and SW_{dif} (full green). Clear sky has been plotted in green. (c) Vegetation canopy resistance r_{veg}, (d) A_n, (e) LE, and (f) SH. These snapshots are instantaneous cross sections of a cloud generated in the REF experiment where (left) depicts 1157 UTC and (center), (right) advances 2 min compared to the previous one.
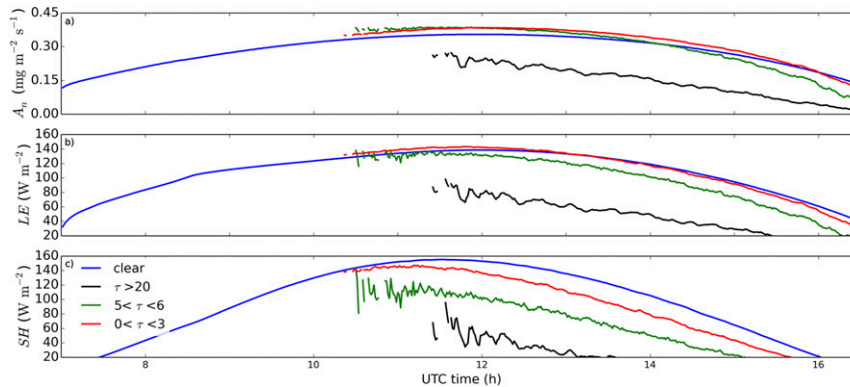
FIG. 3. Time series of (a) A_n, (b) LE, and (c) SH classified according to four conditional averages: clear sky (blue) and three cloud optical depth ranges [$\tau < 3$ (red), $5 < \tau < 6$ (green), and $\tau > 20$ (black)]. The onset of shallow cumulus clouds occurs at 1037 UTC.

evolution of a single cloud in the REF experiment and shows how the surface responds according to the cloud thickness. Figures 2a and 2b illustrate the relation between the cloud optical depth and shortwave radiation, both direct and diffuse. For very thin clouds with $\tau < 3$ (see the area at $x = 400$ m, $y = 750$ m in Fig. 2, left) the decrease in SW$_{dir}$ is to some extent compensated by the increase in SW$_{dif}$. In addition to the known higher penetrative capacity of diffuse radiation inside the canopy (Gu et al. 2003; Knohl and Baldocchi 2008; Urban et al. 2012), more diffuse radiation is created inside the canopy by scattering of leaves (Goudriaan 1977; Baldocchi et al. 1985). The more homogeneous spread of diffuse radiation in the vertical increases the stomatal conductance and decreases the vegetation canopy resistance for water vapor r_{veg} as long as the total radiation at surface does not decrease dramatically (Fig. 2c). This decrease in vegetation resistance due to diffuse radiation is a scale-dependent property. While it is not found at leaf level (Brodersen et al. 2008), this increase is present when we upscale from the leaf to canopy level.

Although the total radiation at the surface is locally reduced compared to cloudless conditions, the higher efficiency of diffuse radiation in the canopy explains the growth in A_n, visible as darker green patches in Fig. 2d. We make a more detailed analysis on the factors driving A_n variations in Fig. 6 (described in greater detail below). Linked to A_n, latent heat flux increases under thin clouds: while plants open their stomata to take up CO_2, releasing water vapor becomes unavoidable. Thus, water and carbon fluxes are related through the stomatal opening.

In the conditions in Fig. 2, r_{veg} is on average larger than r_a. However, spatial variations of r_{veg} are as large as 150 s m^{-1} within the surface shaded by the sampled

cloud, while r_a has a more limited variability of around 40 s m^{-1}, and not corresponding exactly to the cloud shading, since surface horizontal wind and updraft locations largely determine r_a (Sikma et al. 2017, manuscript submitted to *Atmos. For. Meteor.*). Thus, the decrease in r_{veg} due to diffuse radiation drives LE variations. However, LE shows weaker enhancement under the thin parts of the cloud than A_n. This is because the vapor pressure deficit (VPD) is also reduced in the shaded colder surface, thus decreasing the last factor in Eq. (1). Although the stomata opening is also indirectly dependent on VPD, its sensitivity is much weaker, thus not being of much importance for r_{veg} or $r_{veg_{CO_2}}$. Sensible heat flux, depicted in Fig. 2f, shows a decrease for all cloud thicknesses. This is because sensible heat flux is driven by the surface temperature [Eq. (2)], which is governed by total radiation and thus decreases for any cloud. The fact that SH depends on r_a, and not on r_{veg}, explains the less clear patterns in Fig. 2f compared to, for example, LE, for which the effect of cloud shading is clearly discernible. However, A_n and LE actually decrease when the cloud optical depth grows farther (see the area at $x = 400$ m, $y = 500$ m in Fig. 2, right). Under such conditions, direct radiation almost vanishes and the diffuse radiation is insufficient to maintain the clear sky high A_n and LE.

To quantify the changes at the surface along the day, we show the temporal variation in vegetation carbon uptake and surface fluxes under clear skies and for a few cloud optical depth bins in Fig. 3. For thick clouds ($\tau > 20$), both latent and sensible heat fluxes are reduced on average compared to clear sky conditions (Figs. 3b,c), as also found by Lohou and Patton (2014) and Horn et al. (2015). A similar effect is found in net carbon assimilation A_n by vegetation. Relevant for our research is that instantaneously responding vegetation under very thin clouds ($\tau < 3$) has a stronger carbon uptake, by as much

as 9%, compared to that of clear sky conditions until 1630 UTC (Fig. 3a). The photosynthesis rate is enhanced due to the large amount of diffuse radiation (Fig. 1c). Even though total radiation is reduced under any cloud, the higher absorption efficiency of diffuse radiation by canopies overcomes the total reduction in light intensity and decreases the average vegetation resistance by as much as 11% (not shown) at around 1200 UTC. Although r_a increases (by about 4% at 1200 UTC, not shown), the larger reduction in vegetation resistance drives the increased activity of vegetation under very thin clouds. Consequently, we also find a latent heat flux that is marginally larger than under clear sky, provided $\tau < 3$, from 1030 to 1330 UTC. This difference between clear sky and very thin clouds is smaller than for A_n and reaches maximum values of only 4% (see interval between 1030 and 1200 UTC in Fig. 3b) because the VPD is also reduced in the shaded colder surface. Since the sensible heat flux depends only on factors independent of radiation partitioning (air–surface temperature gradient and r_a), it decreases under thin clouds too, as observed in Fig. 2. In other words, the reduction in surface energy by thin clouds is not found in LE, so the sensible heat flux must decrease. Values for intermediate cloud optical depth, with τ between 5 and 6, show similar latent heat flux compared to that under clear skies between 1030 and 1130 UTC, and lower afterward.

To further quantify the dependencies of surface fluxes and net carbon uptake on cloud thickness, Fig. 4 shows 1-h-averaged carbon uptake and latent and sensible heat fluxes as a function of cloud optical depth between 1100 and 1200 UTC for the REF and DIR experiments and normalized by clear sky values. We first define a few relevant concepts. We call enhanced regime to the range of cloud optical depths at which we observe enhanced surface exchange. Threshold τ is defined for each flux as that cloud optical depth for which the flux (LE or A_n) equals its clear sky value. The maximum τ is the cloud optical depth at which we observe maximum values of surface exchange.

The enhanced regimes show that the character of diffuse radiation is able to compensate in A_n and LE for the overall reduction in radiation at the surface for thin clouds. Figure 4b shows that this enhancing effect is not present when all radiation is direct. This confirms the finding that thin clouds enhance carbon uptake and evapotranspiration by providing a favorable combination of direct and diffuse radiation. Vegetation net carbon assimilation in the REF experiment shows larger values (as much as 18%) than under clear sky for cloud optical depth below 9. At $\tau \simeq 9$ we find the threshold τ for A_n. For latent heat flux the enhanced regime is
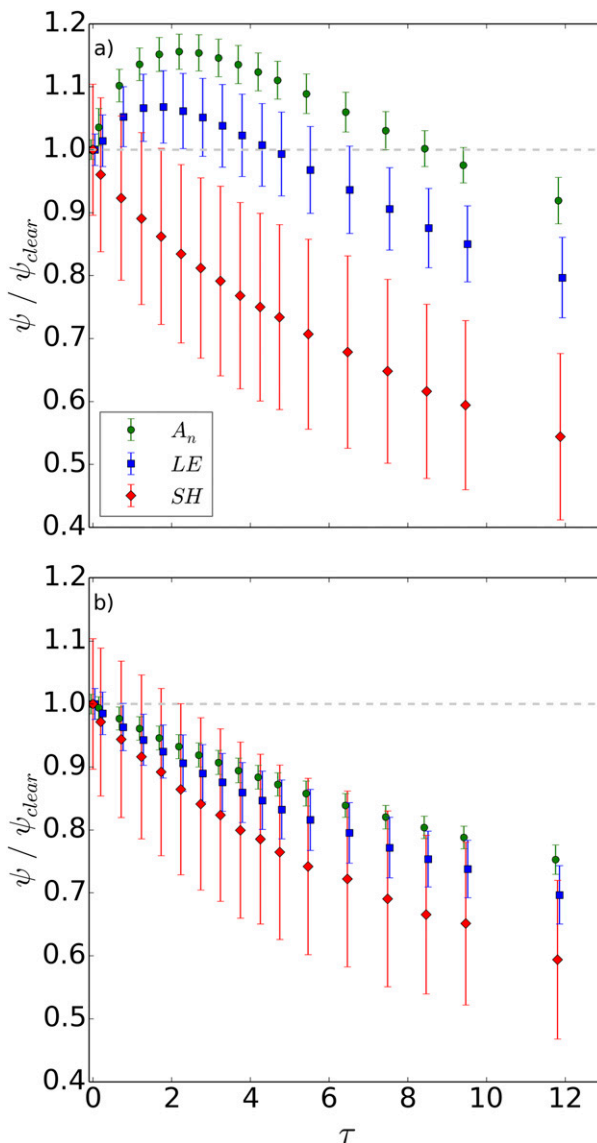

FIG. 4. (a) Mean A_n (green), LE (blue), and SH (red), averaged and binned according to τ between 1100 and 1200 UTC and normalized over clear sky values for the REF experiment. (b) As in (a), but for the DIR experiment. The vertical bar length gives two times the std dev from the mean.

smaller, and its threshold τ is around 4–5. The maximum latent heat flux is about 9% larger than under clear sky. Consistent with what was shown in Fig. 3, the sensible heat flux decreases monotonically with increasing cloud thickness for both cases: as less total radiation reaches the surface, surface temperature decreases and accordingly does the sensible heat flux. Interestingly, the sensible heat flux shows systematic slightly lower values (less than 5%) for the REF case compared to DIR under any cloud due to the increase in LE. This small increase

in SH for the DIR case is interpreted as follows: the additional direct radiation present in DIR instead of the diffuse radiation in REF is not absorbed by the canopy since it does not penetrate that deep in the canopy. Instead, it is directed to light-saturated leaves, decreasing the latent heat flux and increasing the surface temperature and, thus, the sensible heat flux [see Eq. (2)] compared to the REF experiment.

In Fig. 4a an interesting effect is observed: at this time of the day, thin and thick clouds enhance and decrease plant activity, respectively, thus acting in opposing directions regarding surface responses. This means that the presence of thin and thick clouds may lead to similar domain-averaged carbon uptake or surface fluxes in situations where the spatial variability within the domain clearly differs. Note that the thresholds and maximum τ values vary during the day since the solar angle and surface conditions are not constant during the daytime, thus affecting this compensation effect.

For a quantification on the relative changes in Fig. 4, we show the evaporative fraction EF = LE/(LE + SH) and the water use efficiency WUE = A_n/LE, of the REF and DIR experiments in Fig. 5. Regardless of whether radiation has both diffuse and direct components or only direct, both WUE and EF increase under the presence of clouds. A (linear) increase of EF is explained by the more pronounced decline of SH than that of LE when cloud thickness increases regardless of the character of light (Figs. 4a,b). The contribution of diffuse radiation shifts this shape to a more logarithmic-like curve, especially increasing EF for the enhanced regime (Fig. 5a). Since the threshold τ for LE lies around $\tau = 5$, the curve above that cloud thickness in Fig. 5a shows a relative increase similar to that of the DIR experiment. Overall, EF is at least 10% larger for the REF compared to the DIR case under any cloud thickness. This suggests that, considering the entire domain, the EF is positively affected not only by the reduction of total radiation by clouds, as found by Lohou and Patton (2014), but also by the presence of diffuse radiation. The WUE behaves similarly: even for the DIR experiment there is a (linear) growth for increasing τ due to reduction of radiation at surface (Fig. 5b), but the presence of diffuse radiation amplifies the rise in WUE for the enhanced regime $0 < \tau < 8$.

2) Impact on carbon assimilation budget

To disentangle how components in the plant physiological model contribute to the overall increase of carbon assimilation by plants, we perform an offline study using the mixed-layer model CLASS. The conditions for the experiment are set as similar as possible to those of our LES study. In addition, we prescribe the onset,
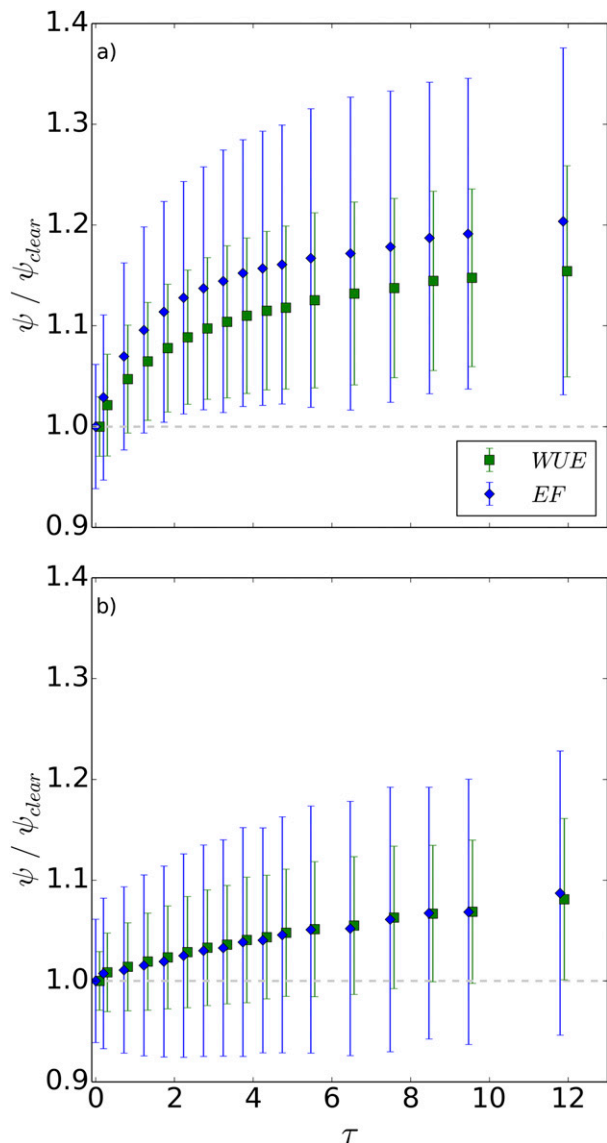

FIG. 5. As in Fig. 4, but for EF and WUE for the (a) REF and (b) DIR experiments.

thickening, and disappearance of a very thin cloud ($\tau = 1$).

The plant physiological model in CLASS is identical to the one used in DALES and described in the supplemental material, and calculates the net carbon uptake at canopy level according to Eq. (3). A budget analysis enables us to understand the contribution of each component of A_n to the cloud-driven change in radiation at the surface around noon for a cloud thickness within the optimum region shown in Fig. 4. It must be noted that we do not intend to characterize the causes and consequences that drive the A_n changes, as the feedbacks and interrelations between plant parameters and variables make such a description quite complex.
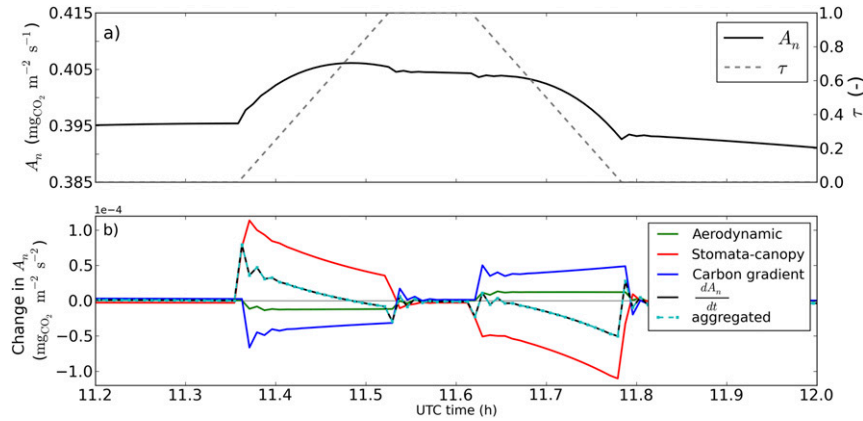
FIG. 6. (a) Net carbon assimilation calculated with CLASS (full line) and prescribed cloud optical depth (dashed line). (b) Time derivative of A_n (black line), aggregate (dashed blue line), and each of the components on the RHS of Eq. (9): carbon gradient (dark blue), aerodynamic (green), and stomata–canopy (red) components as obtained from the CLASS model. The conditions are constrained by the LES results and correspond to average values at 1200 UTC in the REF experiment. Note that a decimal notation is used for time (e.g., 11.5 UTC represents 1130 UTC). This notation also appears in the text where Fig. 6 is discussed.

Instead, with this analysis we aim to depict qualitatively the reaction of the main components in the plant–atmosphere system to fast changes in radiation over time.

The numerator in Eq. (3) represents the CO_2 gradient between the plant and its surrounding environment. The aerodynamic resistance governs the efficiency of transport between leaf and the surrounding atmosphere. This depends on horizontal wind speed (and convective velocity w_* in case of no wind) and is modulated for different stability regimes. Variable $r_{veg_{CO_2}}$ gives the capacity of plant stomata (upscaled at canopy level) to exchange CO_2 with the environment. Since we are interested in the contribution of each factor to the variation in A_n, we differentiate Eq. (3) over time t to obtain a budget with three contributions:

$$\frac{dA_n}{dt} = \underbrace{\frac{1}{r_a + r_{veg_{CO_2}}} \frac{d(C_s - C_i)}{dt}}_{\text{carbon gradient}} - \underbrace{\frac{(C_s - C_i)}{(r_a + r_{veg_{CO_2}})^2} \frac{dr_a}{dt}}_{\text{aerodynamic}} - \underbrace{\frac{(C_s - C_i)}{(r_a + r_{veg_{CO_2}})^2} \frac{dr_{veg_{CO_2}}}{dt}}_{\text{stomata-canopy}}. \tag{9}$$

We name the terms following the derivative in time: plant–atmosphere carbon gradient, aerodynamic, and stomata or canopy resistance terms. The first term on the right-hand side of Eq. (9) represents the change in carbon assimilation due to a variation in the CO_2 gradient between the atmosphere and inside the leaf. An increase (decrease) over time in such a gradient implies an increase (decrease) in carbon assimilation. The second term on the right-hand side accounts for the effect of atmospheric dynamics on the carbon assimilation. Being so, an increase (decrease) in aerodynamic resistance over time, possibly related to a decrease in wind speed or higher atmospheric stability, would decrease (increase) the carbon uptake. The third term on the right-hand side shows the relation between the vegetation resistance to CO_2 transport and A_n. A positive (negative) change in $r_{veg_{CO_2}}$ due to a closing (opening) of stomata in the canopy would decrease (increase) the carbon assimilated by plants.

Figure 6a shows an enhancement in A_n as the cloud optical depth increases, as expected from the optimum range in Fig. 4. The stomatal component is the only term contributing to this enhancement of carbon assimilation when the cloud appears. Since the increase in diffuse radiation compensates for the reduction in total radiation, the vegetation resistance is decreased, lowering the resistance to CO_2 exchange. The colder surface by reduced total radiation decreases the VPD. This decrease correlates with increasing C_i (Jacobs and de Bruin 1997), thus weakening the CO_2 gradient. Thus, the temperature-driven reduction on the CO_2 gradient decreases carbon assimilation or, after adding all components in Eq. (9), decreases the carbon assimilation enhancement driven by the stomata component.

Similarly, although at a smaller scale, the dynamic component hampers the enhanced carbon assimilation. This is due to a decreased total radiation at the surface, which cools the surface and consequently leads to weaker buoyancy flux and related convective motions and thus increases aerodynamic resistance. The symmetric decrease in cloud optical depth after 11.6 UTC shows an analogous impact to that explained for the increasing optical depth, with each factor contributing with opposite sign. For thicker clouds, the temperature-driven negative effects [CO_2 gradient and dynamic components in Eq. (9)] strengthen, while the positive impact of the stomatal component is reduced due to lower total radiation, and it changes sign under thicker clouds. Thus, under thick enough clouds we find a reduction in carbon assimilation.

In the additional DALES experiments, an increase in LAI (from 2 to 5) increases the absorbed radiation by the canopy. The increase is mostly due to the larger number of leaves keeping most of the light inside the canopy. The amount of direct light converted to diffuse light inside the canopy increases with increasing LAI (from 25% to 40% of available direct radiation for LAI = 5), but the direct light converted to diffuse light is not the driving factor for the increased absorbed radiation. In particular, the diffuse radiation causes the latent heat and A_n to rise, while it lowers the sensible heat flux compared to the REF experiment (Fig. 3). However, the differences between clear skies and the cloud thickness bins (Fig. 3 for REF experiment) remain fairly similar. The dependence of surface response to cloud thickness between 1100 and 1200 UTC is very similar to that of Figs. 4a and 5a, with slightly lower EF and larger WUE, but still above clear sky values.

When accounting for the fraction of diffuse radiation (7% of the total radiation) at the top of the boundary layer due to Rayleigh scattering above (AER experiment), we still find an enhanced regime with higher LE and A_n under the (thin) clouds than under cloudless sky. Because there is already some diffuse radiation in clear sky conditions, the threshold and maximum τ are, however, lower than in Fig. 4a. Thus, the relative differences between clouds and clear sky are less pronounced (about 1% lower increase in EF and very similar WUE, not shown).

b. Impact of surface on boundary layer and shallow cumulus

In section 3a(1) it was already shown that the partition between direct and diffuse radiation plays a critical role in the surface response. Therefore, it is interesting to investigate whether these changes at the surface feedback to the boundary layer dynamics and subsequently
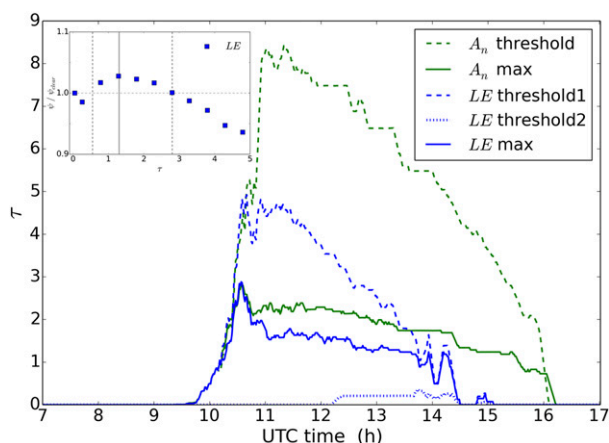

FIG. 7. Cloud optical depth at which values for LE (blue) and A_n (green) are highest (full) and equal to those under clear sky (dashed) in the REF experiment. The dotted line shows the additional threshold τ that appears for LE under very thin clouds in the afternoon (see inset for $0 < \tau < 1$). Inset is as in Fig. 4a, but for instantaneous results at 1300 UTC and only for LE. Vertical dashed gray lines give the two thresholds present at that time, and vertical gray full line the τ at which max LE is found.

to cloud characteristics, such as their formation and vertical development. Focusing on the whole domain, Horn et al. (2015) found significant changes in domain-averaged sensible and latent heat flux when the cloud shading was considered. Yet, they did not quantify the separate contributions of direct and diffuse radiation. Although small spatial variations in surface fluxes are observed starting at the time first clouds develop (1100 UTC), we find that the domain-averaged SH and LE do not change significantly between experiments, as we account for the cloud shading in all our experiments. Domain-averaged vegetation carbon uptake shows larger differences, although still below 5% compared to the REF experiment (not shown).

The reason for smaller differences in evapotranspiration than in A_n is the same as observed in Fig. 3: thin clouds decrease vegetation resistance while cooling the surface. This cooling reduces the VPD, counterbalancing the increase in LE by stomatal opening. Thus, the enhancement compared to clear sky latent heat flux shown in Fig. 4 is, at its maximum, around 10%. This is in contrast to the maximum of 20% found for the vegetation carbon assimilation. Because of the same reason, the enhanced regime is lower for latent heat than for carbon uptake, as already seen for the 1100–1200 UTC average in Fig. 4.

The main reason for the little difference in domain-averaged surface fluxes lies on the limited enhancement of atmosphere–vegetation exchange (less than 10% and 20% at their maxima for LE and A_n, respectively) in the REF experiment. In addition, the threshold τ values are
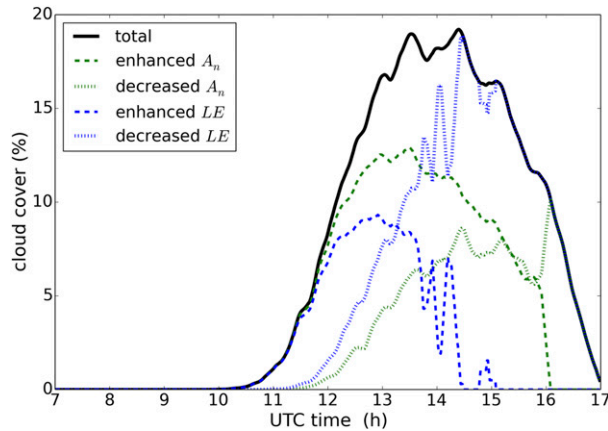
FIG. 8. Total cloud cover (black) and clouded area depending on whether A_n (green) and LE (blue) are enhanced (dashed) or decreased (dotted) compared to clear sky values in the REF experiment. Note that the addition of enhanced and decreased areas equals the total cloud cover except for rounding errors.

dynamic and vary during the day according to solar angle, amount of radiation, and surface conditions such as temperature, CO_2 concentrations, and VPD. Adding the temporal evolution of these thresholds, shown in Fig. 7, to the limited enhancement of A_n and LE limits the duration of the enhanced effect for latent heat and, to a lesser degree, for carbon uptake. Whereas the enhanced regime for A_n is present before 1000 UTC (when first clouds arise) and until after 1600 UTC, the regime for latent heat only lasts between 1000 and 1430 UTC. Moreover, in the afternoon the latent heat under clouds characterized by values $\tau < 1$ is lower compared to clear sky, thus introducing also a lower threshold τ and narrowing the enhancement regime (see inset in Fig. 7). In addition to the limited effect on time and scale, the enhanced latent heat flux and carbon assimilation are also limited in space. The low threshold τ and maximum values for latent heat flux shown in Fig. 7 imply that less of the domain is below clouds with an optical thickness within the enhanced regime. The cloud cover corresponding to the enhanced LE regime is much lower than for the carbon uptake after 1130 UTC (Fig. 8). In fact, after 1430 UTC there is barely any cloud under which enhanced latent heat is found. As for A_n, we find, at its maximum, only 13% of the whole domain to show enhanced A_n (Fig. 8). The compensating effect between thin and thick clouds also limits strong impacts on the atmosphere, as we observe large subareas of the clouded domain, especially in the afternoon and for LE, to decrease the atmosphere–vegetation exchange (Fig. 8). Thus, the effect of enhanced evapotranspiration and carbon uptake due to an optimal combination of diffuse and direct radiation is limited on scale (by limited

maximum values), time (by a limited lifetime of the enhanced regime), and on space (by a low corresponding cloud cover).

Given the very similar response of the surface as a whole to cloud-driven changes in radiation, the boundary layer height evolves almost identically for the three experiments. The boundary layer top starts rising from an initial height of 120 m at sunrise, around 0815 UTC. The appearance of clouds, at around 1000 UTC in our experiments, decelerates the mixed-layer growth by venting air containing high moisture and momentum within the mixed layer to higher levels (Neggers et al. 2006; van Stratum et al. 2014). The maximum boundary layer height, similar for three experiments, reaches around 1950 m at 1630 UTC (not shown). In addition, vertical profiles of potential temperature and specific humidity at the subcloud layer are almost identical between the three experiments. Domain-averaged heat and humidity fluxes along the boundary layer show small differences between experiments and are similar to previous studies (Brown et al. 2002; Siebesma et al. 2003). These findings support the results by Patton et al. (2005), who found little impact of short-scale (i.e., 2 km) surface heterogeneities on vertical flux profiles. In all experiments, first very thin convective clouds appear at around 1000 UTC. As the day evolves, cloud cover increases with shallow clouds growing larger both on horizontal and vertical scales (not shown). In the afternoon, the number of clouds decreases, although the large extension of the remaining ones keeps the cloud cover fairly similar. The cloud cover oscillates around a maximum value of almost 20% in the afternoon for the three experiments (Fig. 8 for REF), and we find a similar maximum cloud area fraction (the maximum cloud cover in a single vertical level) and maximum cloud core area fraction for the different experiments, thus suggesting that the strength of updrafts and mass flux within the clouds is not affected by changes at the surface.

The three-dimensional conditional averaging method for clouds presented in section 2d allows us to carry out a much more detailed and precise analysis on the characteristics of clouds. In Fig. 9a we show the water content of cloud and cloud cores between 1400 and 1420 UTC in the REF, DIR, and DIF experiments when the cloud cover is maximum. All experiments show a larger content on cloud cores than in clouds, as already documented in literature (Siebesma et al. 2003; Zhao and Austin 2005). The direct or diffuse character of light does not affect the properties of clouds, as shown in Fig. 9a. The differences between experiments in q_l are on the order of the standard deviations within each experiment: below 4000 m differences between experiments reach maximum values of $0.15 \, \mathrm{g \, kg^{-1}}$, while the
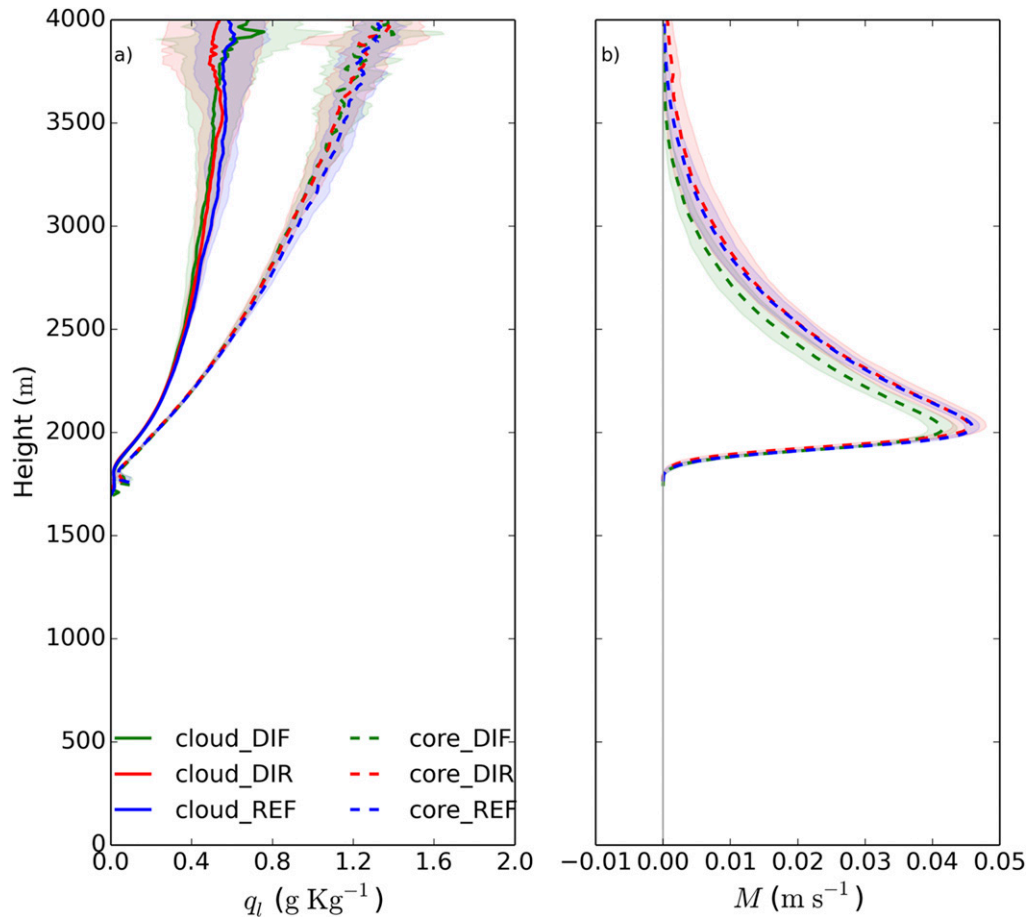
FIG. 9. Conditional average on clouds (full) and cloud cores (dashed) of (left) liquid water mixing ratio and (right) mass flux for the REF (blue), DIR (red), and DIF (green) experiments. The profiles have been averaged between 1400 and 1420 UTC. Std dev for the temporal average is shaded.

standard deviation within each experiment is almost double the relative differences between experiments. In Fig. 9b we observe that the mass flux vertical profile by cloud cores, that is, the additional vertical velocity induced by the presence of clouds (Heus and Jonker 2008; Ouwersloot et al. 2013), is similar between these experiments. It shows a maximum at around 2000 m, which coincides with the maximum cloud core area at the same time (not shown). The small difference in the DIF experiment is due to the limitation of the domain extension and can disappear or even change sign depending on the averaging time. All three experiments show a similar evolution of the maximum mass flux during the day (not shown).

The differences in treatment of radiation between the experiments allow us to give an indication for future parameterizations: while the partitioning of diffuse and direct components has some impact at the surface, locally affecting the surface fluxes and vegetation performance, it does not noticeably impact the dynamics of the boundary layer and the formation of low convective clouds.

The additional LAI5 experiment yields a lower boundary layer, cloud height, and slightly larger water content on clouds (not shown) than for lower LAI (REF experiment). These differences are driven by the larger transpiration due to a denser canopy. Although domain-averaged surface fluxes are very similar between AER and REF, all clouds after 1300 UTC reduce the latent heat flux compared to clear sky in AER. This is due to the very narrow enhanced regime for LE in AER. We find a slightly lower ABL height and very similar cloud cover and cloud characteristics for this additional experiment.

4. Summarized conclusions and recommendations

By coupling radiation, surface and turbulence processes in the Dutch Atmospheric Large-Eddy Simulation (DALES), we study the effects of direct and diffuse

radiation in a diurnal boundary layer over vegetation. We pay special attention to how the direct and diffuse partitioning perturbed by clouds is further disturbed in the canopy, modifying photosynthesis, plant evapotranspiration, and sensible heat flux. We design three idealized experiments to clarify the role of diffuse and direct radiation at the vegetated canopy, boundary layer, and clouds under free convective conditions (no mean horizontal wind). To disentangle the effects of cloud thickness on direct and diffuse radiation, we apply a conditional averaging at the surface dependent on the cloud optical depth above.

By calculating the radiative transfer in clouds with the delta-Eddington radiative scheme, we find a decrease in total radiation at the surface under all cloud thicknesses. The fraction of diffuse radiation, however, increases for thin clouds and peaks at values of cloud optical depth between 1 and 8, typical values for shallow cumulus clouds. The sensitivity of radiation to cloud optical depth leads to different partitions of direct and diffuse radiation at the canopy top, which has an impact on the transfer of radiation inside the canopy, as diffuse radiation has larger penetrative capacity. In consequence, vegetation resistance is reduced under very thin clouds (as much as 11% at 1200 UTC), thus allowing for a larger exchange of water vapor (latent heat flux) and CO_2 (vegetation carbon assimilation). We find a compensating effect between thin and thick clouds over the domain: thin clouds enhance the latent heat flux and photosynthesis, whereas thick clouds decrease them. Diffuse radiation from clouds is also responsible for the photosynthesis-driven increase in water use efficiency and evaporative fraction compared to the case when all radiation is direct.

To support the DALES results, we perform an offline analysis using an atmospheric mixed-layer model to isolate and break up the complexity on the response of vegetation to prescribed cloud shading. We find changes in stomatal opening to lead the increased carbon uptake under very thin clouds. The CO_2 gradient between the leaf and its environment and the aerodynamic resistance are of secondary relevance. Yet, they effectively reduce the enhancement of carbon uptake under very thin clouds.

As for the impact of dynamic surface heterogeneities on the boundary layer structures, diffuse radiation does not play a relevant role in our experiments: similar domain-averaged latent and sensible heat fluxes, boundary layer heights, and cloud characteristics are found regardless of the character of radiation under clouds. Slightly larger differences are found for domain-averaged carbon uptake, although below 5%. The reduced difference in domain-averaged responses to diffuse radiation has several reasons. At its maximum,

the latent heat flux and carbon assimilation enhancement is 10% and 20% for thin clouds. In addition, the regime for cloud thickness under which we observe an enhanced exchange is restricted and short lived. As a consequence, we observe a smaller area over which the enhanced evapotranspiration and carbon uptake are present (a maximum of 8% and 13% of the whole surface, respectively). In addition, the area under which latent heat flux and carbon uptake are reduced is comparable or larger than the enhanced area, especially in the afternoon, thus compensating the effect of thin clouds by thick clouds. All factors combined limit the sensitivity of domain-averaged boundary layer and cloud dynamics to direct and diffuse radiation.

We extend our study by performing sensitivity analysis to various canopy conditions (LAI) and atmospheric conditions (background diffuse radiation). It is found that an increase in LAI, in our study from 2 to 5, raises evapotranspiration, thus lowering boundary layer and cloud-base height and slightly increasing the water content on clouds. However, the increase in LAI does not change the sensitivity of the canopy to cloud optical properties. In the experiment accounting for background diffuse radiation, the enhanced activity under thin clouds is dampened, but the main features of the reference experiment remain.

Our findings invite investigations under a wider range of meteorological and plant conditions. The response of vegetation is very likely to change under water-stress conditions or different temperature or water content in the atmosphere. A more realistic behavior of plants would include a gradual response of stomata to changing light conditions, which may affect the surface fluxes. Further research should include the variations in longwave radiation due to clouds, as they may lay on the order of the enhanced and decreased surface fluxes due to shading. In addition, a study of the shaded surface, paying attention to local vertical motions, could provide a more complete understanding of the local effects of diffuse radiation in the boundary layer. Numerical experiments with background wind or a more realistic (noninstantaneous) light response of vegetation would contribute to the understanding on the role of diffuse radiation. An assessment of the sensitivity of our results to the leaf angle distribution in the plant physiological model would be of interest for a better understanding of the role of the canopy in the system. Furthermore, the low cloud cover characteristic of shallow cumulus situations (maximum of 20% and restricted to less than 3 h in this study) limits the impact of cloud-dependent surface fluxes on the boundary layer. Thus, different results are possible on more sensitive cases, such as a boundary layer topped by stratocumulus.

The optical depths of stratocumulus are usually constrained to $\tau < 20$ and do not reach locally as high values as those for certain shallow cumulus, while the cloud cover can be much larger than in our study. Although in stratocumulus clouds the updrafts are not the trigger for clouds, they do play a role in the evolution of the cloud layer and its breakup. Thus, diffuse and direct radiation partition may be relevant in the evolution of a stratocumulus-topped boundary layer. Finally, our results, located in midlatitudes, may differ from those closer to the equator with smaller zenith angles, and thus larger amounts of diffuse radiation for thin clouds, as well as a wider range of cloud optical depths with significant diffuse radiation.

REFERENCES

Avissar, R., and T. Schmidt, 1998: An evaluation of the scale at which ground-surface heat flux patchiness affects the convective boundary layer using large-eddy simulations. *J. Atmos. Sci.*, **55**, 2666–2689, doi:10.1175/1520-0469(1998)055<2666:AEOTSA>2.0.CO;2.

Baker, M. B., and J. Latham, 1979: The evolution of droplet spectra and the rate of production of embryonic raindrops in small cumulus clouds. *J. Atmos. Sci.*, **36**, 1612–1615, doi:10.1175/1520-0469(1979)036<1612:TEODSA>2.0.CO;2.

Baldocchi, D., and S. Ma, 2013: How will land use affect air temperature in the surface boundary layer? Lessons learned from a comparative study on the energy balance of an oak savanna and annual grassland in California, USA. *Tellus*, **65B**, 19994, doi:10.3402/tellusb.v65i0.19994.

——, B. A. Hutchison, D. R. Matt, and R. T. McMillen, 1985: Canopy radiative transfer models for spherical and known leaf inclination angle distributions: A test in an oak–hickory forest. *J. Appl. Ecol.*, **22**, 539–555, doi:10.2307/2403184.

Barbaro, E., 2015: Interaction between aerosols and convective boundary-layer dynamics over land. Ph.D. thesis, Wageningen University, 193 pp. [Available online at http://edepot.wur.nl/335853.]

——, J. V.-G. de Arellano, H. G. Ouwersloot, J. S. Schrter, D. P. Donovan, and M. C. Krol, 2014: Aerosols in the convective boundary layer: Shortwave radiation effects on the coupled land–atmosphere system. *J. Geophys. Res. Atmos.*, **119**, 5845–5863, doi:10.1002/2013JD021237.

Betts, A. K., 1973: Non-precipitating cumulus convection and its parameterization. *Quart. J. Roy. Meteor. Soc.*, **99**, 178–196, doi:10.1002/qj.49709941915.

——, M. Goulden, and S. Wofsy, 1999: Controls on evaporation in a boreal spruce forest. *J. Climate*, **12**, 1601–1618, doi:10.1175/1520-0442(1999)012<1601:COEIAB>2.0.CO;2.

Böing, S. J., H. J. J. Jonker, A. P. Siebesma, and W. W. Grabowski, 2012: Influence of the subcloud layer on the development of a deep convective ensemble. *J. Atmos. Sci.*, **69**, 2682–2698, doi:10.1175/JAS-D-11-0317.1.

Boussetta, S., and Coauthors, 2013: Natural land carbon dioxide exchanges in the ECMWF Integrated Forecasting System: Implementation and offline validation. *J. Geophys. Res. Atmos.*, **118**, 5923–5946, doi:10.1002/jgrd.50488.

Brodersen, C. R., T. C. Vogelmann, W. E. Williams, and H. L. Gorton, 2008: A new paradigm in leaf-level photosynthesis: Direct and diffuse lights are not equal. *Plant Cell Environ.*, **31**, 159–164, doi:10.1111/j.1365-3040.2007.01751.x.

Brown, A. R., and Coauthors, 2002: Large-eddy simulation of the diurnal cycle of shallow cumulus convection over land. *Quart. J. Roy. Meteor. Soc.*, **128**, 1075–1093, doi:10.1256/003590002320373210.

Cheng, S. J., A. L. Steiner, D. Y. Hollinger, G. Bohrer, and K. J. Nadelhoffer, 2016: Using satellite-derived optical thickness to assess the influence of clouds on terrestrial carbon uptake. *J. Geophys. Res. Biogeosci.*, **121**, 1747–1761, doi:10.1002/2016JG003365.

Chlond, A., O. Boehringer, T. Auerswald, and F. Mueller, 2014: The effect of soil moisture and atmospheric conditions on the development of shallow cumulus convection: A coupled large-eddy simulation–land surface model study. *Meteor. Z.*, **23**, 491–510, doi:10.1127/metz/2014/0576.

De Bruin, H. A. R., and Coauthors, 1989: Forests and regional-scale processes. *Philos. Trans. Roy. Soc. London*, **324B**, 393–406, doi:10.1098/rstb.1989.0054.

Esau, I., and T. Lyons, 2002: Effect of sharp vegetation boundary on the convective atmospheric boundary layer. *Agric. For. Meteor.*, **114**, 3–13, doi:10.1016/S0168-1923(02)00154-5.

Freedman, J. M., D. R. Fitzjarrald, K. E. Moore, and R. K. Sakai, 2001: Boundary layer clouds and vegetation–atmosphere feedbacks. *J. Climate*, **14**, 180–197, doi:10.1175/1520-0442(2001)013<0180:BLCAVA>2.0.CO;2.

Garcia-Carreras, L., D. J. Parker, C. M. Taylor, C. E. Reeves, and J. G. Murphy, 2010: Impact of mesoscale vegetation heterogeneities on the dynamical and thermodynamic properties of the planetary boundary layer. *J. Geophys. Res.*, **115**, D03102, doi:10.1029/2009JD012811.

——, ——, and J. H. Marsham, 2011: What is the mechanism for the modification of convective cloud distributions by land surface–induced flows? *J. Atmos. Sci.*, **68**, 619–634, doi:10.1175/2010JAS3604.1.

Golaz, J.-C., H. Jiang, and W. R. Cotton, 2001: A large-eddy simulation study of cumulus clouds over land and sensitivity to soil moisture. *Atmos. Res.*, **59–60**, 373–392, doi:10.1016/S0169-8095(01)00113-2.

Goudriaan, J., 1977: Crop micrometeorology: A simulation study. Ph.D. thesis, Wageningen University, 249 pp. [Available online at http://edepot.wur.nl/166537.]

——, 1986: A simple and fast numerical method for the computation of daily totals of crop photosynthesis. *Agric. For. Meteor.*, **38**, 249–254, doi:10.1016/0168-1923(86)90063-8.

Gronemeier, T., F. Kanani-Sühring, and S. Raasch, 2017: Do shallow cumulus clouds have the potential to trigger secondary circulations via shading? *Bound.-Layer Meteor.*, **162**, 143–169, doi:10.1007/s10546-016-0180-7.

Gu, L., D. D. Baldocchi, S. C. Wofsy, J. W. Munger, J. J. Michalsky, S. P. Urbanski, and T. A. Boden, 2003: Response of a

deciduous forest to the Mount Pinatubo eruption: Enhanced photosynthesis. *Science*, **299**, 2035–2038, doi:10.1126/science.1078366.

Heus, T., and Coauthors, 2010: Formulation of the Dutch Atmospheric Large-Eddy Simulation (DALES) and overview of its applications. *Geosci. Model Dev.*, **3**, 415–444, doi:10.5194/gmd-3-415-2010.

——, and H. J. J. Jonker, 2008: Subsiding shells around shallow cumulus clouds. *J. Atmos. Sci.*, **65**, 1003–1018, doi:10.1175/2007JAS2322.1.

Horn, G. L., H. G. Ouwersloot, J. Vilà-Guerau de Arellano, and M. Sikma, 2015: Cloud shading effects on characteristic boundary-layer length scales. *Bound.-Layer Meteor.*, **157**, 237–263, doi:10.1007/s10546-015-0054-4.

Huang, H.-Y., and S. A. Margulis, 2010: Evaluation of a fully coupled large-eddy simulation–land surface model and its diagnosis of land–atmosphere feedbacks. *Water Resour. Res.*, **46**, W06512, doi:10.1029/2009WR008232.

Jacobs, C. M. J., and H. A. R. de Bruin, 1997: Predicting regional transpiration at elevated atmospheric CO_2: Influence of the PBL–vegetation interaction. *J. Appl. Meteor.*, **36**, 1663–1675, doi:10.1175/1520-0450(1997)036<1663:PRTAEA>2.0.CO;2.

——, B. van den Hurk, and H. de Bruin, 1996: Stomatal behaviour and photosynthetic rate of unstressed grapevines in semi-arid conditions. *Agric. For. Meteor.*, **80**, 111–134, doi:10.1016/0168-1923(95)02295-3.

Joseph, J. H., W. J. Wiscombe, and J. A. Weinman, 1976: The delta-Eddington approximation for radiative flux transfer. *J. Atmos. Sci.*, **33**, 2452–2459, doi:10.1175/1520-0469(1976)033<2452:TDEAFR>2.0.CO;2.

Kanniah, K. D., J. Beringer, P. North, and L. Hutley, 2012: Control of atmospheric particles on diffuse radiation and terrestrial plant productivity: A review. *Prog. Phys. Geogr.*, **36**, 209–237, doi:10.1177/0309133311434244.

Knohl, A., and D. D. Baldocchi, 2008: Effects of diffuse radiation on canopy gas exchange processes in a forest ecosystem. *J. Geophys. Res.*, **113**, G02023, doi:10.1029/2007JG000663.

Lohou, F., and E. G. Patton, 2014: Surface energy balance and buoyancy response to shallow cumulus shading. *J. Atmos. Sci.*, **71**, 665–682, doi:10.1175/JAS-D-13-0145.1.

Lu, C., S. Niu, Y. Liu, and A. M. Vogelmann, 2013: Empirical relationship between entrainment rate and microphysics in cumulus clouds. *Geophys. Res. Lett.*, **40**, 2333–2338, doi:10.1002/grl.50445.

McFarlane, S. A., and W. W. Grabowski, 2007: Optical properties of shallow tropical cumuli derived from arm ground-based remote sensing. *Geophys. Res. Lett.*, **34**, L06808, doi:10.1029/2006GL028767.

Min, Q., 2005: Impacts of aerosols and clouds on forest–atmosphere carbon exchange. *J. Geophys. Res.*, **110**, D06203, doi:10.1029/2004JD004858.

——, and S. Wang, 2008: Clouds modulate terrestrial carbon uptake in a midlatitude hardwood forest. *Geophys. Res. Lett.*, **35**, L02406, doi:10.1029/2007GL032398.

Neggers, R., B. Stevens, and J. D. Neelin, 2006: A simple equilibrium model for shallow-cumulus-topped mixed layers. *Theor. Comput. Fluid Dyn.*, **20**, 305–322, doi:10.1007/s00162-006-0030-1.

Nieuwstadt, F. T. M., and R. A. Brost, 1986: The decay of convective turbulence. *J. Atmos. Sci.*, **43**, 532–546, doi:10.1175/1520-0469(1986)043<0532:TDOCT>2.0.CO;2.

Norman, J., 1979: Modeling the complete crop canopy. *Modification of the Aerial Environment of Crops*, B. J. Barfield and J. F.

Gerber, Eds., American Society of Agricultural Engineers, 249–280.

Oliphant, A., D. Dragoni, B. Deng, C. Grimmond, H.-P. Schmid, and S. Scott, 2011: The role of sky conditions on gross primary production in a mixed deciduous forest. *Agric. For. Meteor.*, **151**, 781–791, doi:10.1016/j.agrformet.2011.01.005.

Oliveira, P. J. C., E. L. Davin, S. Levis, and S. I. Seneviratne, 2011: Vegetation-mediated impacts of trends in global radiation on land hydrology: A global sensitivity study. *Global Change Biol.*, **17**, 3453–3467, doi:10.1111/j.1365-2486.2011.02506.x.

Ouwersloot, H. G., J. Vilà-Guerau de Arellano, C. C. van Heerwaarden, L. N. Ganzeveld, M. C. Krol, and J. Lelieveld, 2011: On the segregation of chemical species in a clear boundary layer over heterogeneous land surfaces. *Atmos. Chem. Phys.*, **11**, 10 681–10 704, doi:10.5194/acp-11-10681-2011.

——, J. V.-G. de Arellano, B. J. H. van Stratum, M. C. Krol, and J. Lelieveld, 2013: Quantifying the transport of subcloud layer reactants by shallow cumulus clouds over the Amazon. *J. Geophys. Res. Atmos.*, **118**, 13 041–13 059, doi:10.1002/2013JD020431.

——, A. F. Moene, J. J. Attema, and J. V.-G. de Arellano, 2017: Large-eddy simulation comparison of neutral flow over a canopy: Sensitivities to physical and numerical conditions, and similarity to other representations. *Bound.-Layer Meteor.*, **162**, 71–89, doi:10.1007/s10546-016-0182-5.

Patton, E. G., P. P. Sullivan, and C.-H. Moeng, 2005: The influence of idealized heterogeneity on wet and dry planetary boundary layers coupled to the land surface. *J. Atmos. Sci.*, **62**, 2078–2097, doi:10.1175/JAS3465.1.

Ronda, R. J., H. A. R. de Bruin, and A. A. M. Holtslag, 2001: Representation of the canopy conductance in modeling the surface energy budget for low vegetation. *J. Appl. Meteor.*, **40**, 1431–1444, doi:10.1175/1520-0450(2001)040<1431:ROTCCI>2.0.CO;2.

Schumann, U., A. Dörnbrack, and B. Mayer, 2002: Cloud-shadow effects on the structure of the convective boundary layer. *Meteor. Z.*, **11**, 285–294, doi:10.1127/0941-2948/2002/0011-0285.

Schwartz, S. E., D. Huang, and D. V. Vladutescu, 2017: High-resolution photography of clouds from the surface: Retrieval of optical depth of thin clouds down to centimeter scales. *J. Geophys. Res. Atmos.*, **122**, 2898–2928, doi:10.1002/2016JD025384.

Shettle, E. P., and J. A. Weinman, 1970: The transfer of solar irradiance through inhomogeneous turbid atmospheres evaluated by Eddington's approximation. *J. Atmos. Sci.*, **27**, 1048–1055, doi:10.1175/1520-0469(1970)027<1048:TTOSIT>2.0.CO;2.

Siebesma, A. P., and Coauthors, 2003: A large eddy simulation intercomparison study of shallow cumulus convection. *J. Atmos. Sci.*, **60**, 1201–1219, doi:10.1175/1520-0469(2003)60<1201:ALESIS>2.0.CO;2.

Sikma, M., and H. G. Ouwersloot, 2015: Parameterizations for convective transport in various cloud-topped boundary layers. *Atmos. Chem. Phys.*, **15**, 10 399–10 410, doi:10.5194/acp-15-10399-2015.

Slawinska, J., W. W. Grabowski, H. Pawlowska, and A. A. Wyszogrodzki, 2008: Optical properties of shallow convective clouds diagnosed from a bulk-microphysics large-eddy simulation. *J. Climate*, **21**, 1639–1647, doi:10.1175/2007JCLI1820.1.

Spitters, C., 1986: Separating the diffuse and direct component of global radiation and its implications for modeling canopy photosynthesis Part II. Calculation of canopy photosynthesis. *Agric. For. Meteor.*, **38**, 231–242, doi:10.1016/0168-1923(86)90061-4.

Stephens, G. L., 1984: The parameterization of radiation for numerical weather prediction and climate models. *Mon. Wea.*

Rev., **112**, 826–867, doi:10.1175/1520-0493(1984)112<0826:TPORFN>2.0.CO;2.

Urban, O., and Coauthors, 2012: Impact of clear and cloudy sky conditions on the vertical distribution of photosynthetic CO_2 uptake within a spruce canopy. *Funct. Ecol.*, **26**, 46–55, doi:10.1111/j.1365-2435.2011.01934.x.

van Heerwaarden, C. C., J. Vilà-Guerau de Arellano, A. F. Moene, and A. A. M. Holtslag, 2009: Interactions between dry-air entrainment, surface evaporation and convective boundary-layer development. *Quart. J. Roy. Meteor. Soc.*, **135**, 1277–1291, doi:10.1002/qj.431.

——, ——, A. Gounou, F. Guichard, and F. Couvreux, 2010: Understanding the daily cycle of evapotranspiration: A method to quantify the influence of forcings and feedbacks. *J. Hydrometeor.*, **11**, 1405–1422, doi:10.1175/2010JHM1272.1.

van Stratum, B. J. H., J. Vilà-Guerau de Arellano, C. C. van Heerwaarden, and H. G. Ouwersloot, 2014: Subcloud-layer feedbacks driven by the mass flux of shallow cumulus convection over land. *J. Atmos. Sci.*, **71**, 881–895, doi:10.1175/JAS-D-13-0192.1.

Vilà-Guerau de Arellano, J., C. C. van Heerwaarden, and J. Lelieveld, 2012: Modelled suppression of boundary-layer clouds by plants in a CO_2-rich atmosphere. *Nat. Geosci.*, **5**, 701–704, doi:10.1038/ngeo1554.

——, H. G. Ouwersloot, D. Baldocchi, and C. M. J. Jacobs, 2014: Shallow cumulus rooted in photosynthesis. *Geophys. Res. Lett.*, **41**, 1796–1802, doi:10.1002/2014GL059279.

——, C. C. van Heerwaarden, B. J. van Stratum, and K. van den Dries, 2015: *Atmospheric Boundary Layer: Integrating Air Chemistry and Land Interactions.* Cambridge University Press, 276 pp., doi:10.1017/CBO9781316117422.

Wang, K., R. E. Dickinson, and S. Liang, 2008: Observational evidence on the effects of clouds and aerosols on net ecosystem exchange and evapotranspiration. *Geophys. Res. Lett.*, **35**, L10401, doi:10.1029/2008GL034167.

Yu, H., S. C. Liu, and R. E. Dickinson, 2002: Radiative effects of aerosols on the evolution of the atmospheric boundary layer. *J. Geophys. Res.*, **107**, 4142, doi:10.1029/2001JD000754.

Zhao, M., and P. H. Austin, 2005: Life cycle of numerically simulated shallow cumulus clouds. Part I: Transport. *J. Atmos. Sci.*, **62**, 1269–1290, doi:10.1175/JAS3414.1.